PHYSOR 2004 -The Physics of Fuel Cycles and Advanced Nuclear Systems: Global Developments
Chicago, Illinois, April 25-29, 2004, on CD-ROM, American Nuclear Society, Lagrange Park, IL. (2004)

MINERVE Reactor Characterization in Support of the OSMOSE Program: Safety parameters

Jean-Pascal HUDELOT[2], Raymond KLANN[1], Bradley MICKLICH[1], Muriel ANTONY[2], Gregory PERRET[1], Nicolas THIOLLAY[2], Jean-Michel GIRARD[2], Valerie LAVAL[2], Pierre LECONTE[2]

[1]Argonne National Laboratory, 9700 South Cass Avenue, Argonne, IL 60439, USA
[2]CEA Cadarache, DEN/DER, 13108 Saint Paul lez Durance, France

The experimental reactor MINERVE is devoted to neutronic studies of lattices of different reactor types. MINERVE is a pool type reactor operating at a maximum power of 100 W. The core, submerged under 3 meters of water, is used as a driver zone for the different experiments located in a central square cavity with a size of about 70 cm × 70 cm. The coupled lattices in this cavity are built in such a way that they can reproduce the neutronic spectra of a fast reactor, a light water reactor, a RSM reactor and a heavy water reactor. It provides a large experimental basis for the improvement of the cross section databases. An oscillation technique is used to determine the reactivity worth of samples containing the material of interest: actinides, absorbers, poisons, spent fuel, structural materials, etc.

An ambitious program between the Commissariat à l'Energie Atomique (CEA) and the U.S. Department of Energy (DOE) has been launched with the aim of measuring the integral absorption rate parameters of actinide isotopes in the MINERVE experimental facility located at the CEA Cadarache Research Center. The OSMOSE Program (OScillation in Minerve of isOtopes in "Eupraxic" Spectra) includes a complete analytical program associated with the experimental measurement program and aims at understanding and resolving potential discrepancies between calculated and measured values for the studied actinides.

Before beginning the experimental measurements, it is necessary to prove that it is possible to accurately predict the safety parameters for the reactor operation and to effectively control the reactor during experimental measurements. In this context, a significant effort is underway to model the reactor, to calculate relevant safety parameters, and to conduct measurements using the MINERVE reactor to obtain values for the safety parameters.

For the safe operation of the reactor, it is vital to fully understand the criticality parameters of the core, including the multiplication factor, the reactivity worth of the control rods (measured by rod drop technique), the critical position of the rods and the reactivity excess of the core (obtained by doubling-time measurement).

Another parameter being studied is the axial profile of the reaction rate in the central channel of the lattice. This channel is the location where the OSMOSE samples will be oscillated for the experimental measurements so it is vital to understand the flux profile in this region. The axial shaping factor is used in

the absolute power calibration of the reactor, and therefore, it is important to accurately determine the spatial flux profile. Experiments are performed by integral gamma-spectroscopy to provide the total fission rate axial profile, and with miniature fission chambers to measure the axial profile of ^{237}Np and ^{235}U fission rates. Results from the experiments and compared to calculations of these parameters.

Finally, the radial power profile inside the experimental region is also being studied. The radial power profile provides information on the radial shaping factor and also must be known with reasonable accuracy because it is used in the absolute power calibration of the reactor. Experimental results are obtained using integral gamma-scanning to determine the relative power in the UO_2 zone and MOX zone within the R1-MOX lattice and are based on single peak gamma scanning on ^{140}La gamma-ray at 1596 keV. These results are used to compare and normalize the UO_2 zone and MOX zone power distributions. MCNP modeling is used to compute the power profile for the experimental region.

KEYWORDS: rod drop, reactivity worth, OSMOSE, MINERVE, actinides, fission chambers, gamma spectroscopy, MCNP,TRIPOLI4, axial buckling, radial power profile, multiplication factor

1. Introduction

The experimental reactor MINERVE is devoted to neutronic studies of lattices of different reactor types. MINERVE is a pool type reactor operating at a maximum power of 100 W. The core, submerged under 3 meters of water, is used as a driver zone for the different experiments located in a central square cavity with a size of about 70 cm × 70 cm. The coupled lattices in this cavity are built in such a way that they can reproduce the neutronic spectra of a fast reactor, a light water reactor, a RSM reactor and a heavy water reactor. MINERVE achieved its first criticality in 1959 in CEA Fontenay-aux-Roses (near Paris). The reactor was then transferred to Cadarache in 1977. The driver zone consists of enriched metallic uranium/aluminium plates cladded with aluminium and gathered in *MTR* elements of 9, 12 and 18 plates. About 30 elements compose the driver zone which is surrounded by a graphite reflector. The thermal flux is about 10^9 n/cm²/s at a power level of 100 Watts. The reactor is controlled using 4 hafnium rods.

MINERVE provides a large experimental basis for the improvement of the cross section databases. An oscillation technique is used to determine the reactivity worth of samples containing the material of interest: actinides, absorbers, poisons, spent fuel, structural materials, etc.

An ambitious program between the Commissariat à l'Energie Atomique (CEA) and the U.S. Department of Energy (DOE) has been launched with the aim of measuring the integral absorption rate parameters of actinide isotopes in the MINERVE experimental facility located at the CEA Cadarache Research Center. The OSMOSE Program (OScillation in Minerve of isOtopes in "Eupraxic" Spectra) includes a complete analytical program associated with the experimental measurement program and aims at understanding and resolving potential discrepancies between calculated and measured values for the studied actinides.

Before beginning the experimental measurements, it is necessary to prove that it is possible to accurately predict the safety parameters for the reactor operation and to effectively control the reactor during experimental measurements. In this context, a significant effort is underway to model the reactor, to calculate relevant safety parameters, and to conduct measurements using the MINERVE reactor to obtain values for the safety parameters.

The use of future core loadings in MINERVE requires updated calculations of safety parameters with an improved accuracy, in order to address safety authorization requirements. This is also necessary because of the decay of MOX fuel with time (MOX fuel is 30 years old) and because of maintenance and upgrades to MINERVE in 2002 that aimed at improving the reliability and the accuracy of the facility and the experiments.

The MINERVE reactor facility and experimental configurations are described in two other papers [1,2] and are not repeated here. This paper describes the results of the reactor modeling and provides a comparison of calculations to initial experiments performed on the MINERVE facility for parameters important for safety authorization. Two different core configurations were used for the measurements: R1-UO2, representative of a PWR spectrum (lattice of 3% enriched UO2 fuel pins), and R1-MOX, representative of a MOX-PWR spectrum (lattice of UO2 and MOX fuel pins containing 3.6% and 4% plutonium and 3% enriched UO2 fuel pins).

For the safe operation of the reactor, it is vital to fully understand the criticality parameters of the core, including the multiplication factor, the reactivity worth of the control rods (measured by rod drop technique), the critical position of the rods and the reactivity excess of the core (obtained by doubling-time measurement).

Another parameter being studied is the axial profile of the reaction rate in the central channel of the lattice. This channel is the location where the OSMOSE samples will be oscillated for the experimental measurements so it is vital to understand the flux profile in this region. The axial shaping factor is used in the absolute power calibration of the reactor, and therefore, it is important to accurately determine the spatial flux profile. Experiments are performed by integral gamma-spectroscopy to provide the total fission rate axial profile, and with miniature fission chambers to measure the axial profile of ^{237}Np and ^{235}U fission rates. Results from the experiments and compared to calculations of these parameters.

Finally, the radial power profile inside the experimental region is also being studied. The radial power profile provides information on the radial shaping factor and also must be known with reasonable accuracy because it is used in the absolute power calibration of the reactor. Experimental results are obtained using integral gamma-scanning to determine the relative power in the UO_2 zone and MOX zone within the R1-MOX lattice and are based on single peak gamma scanning on ^{140}La gamma-ray at 1596 keV. These results are used to compare and normalize the UO_2 zone and MOX zone power distributions. MCNP modeling is used to compute the power profile for the experimental region.

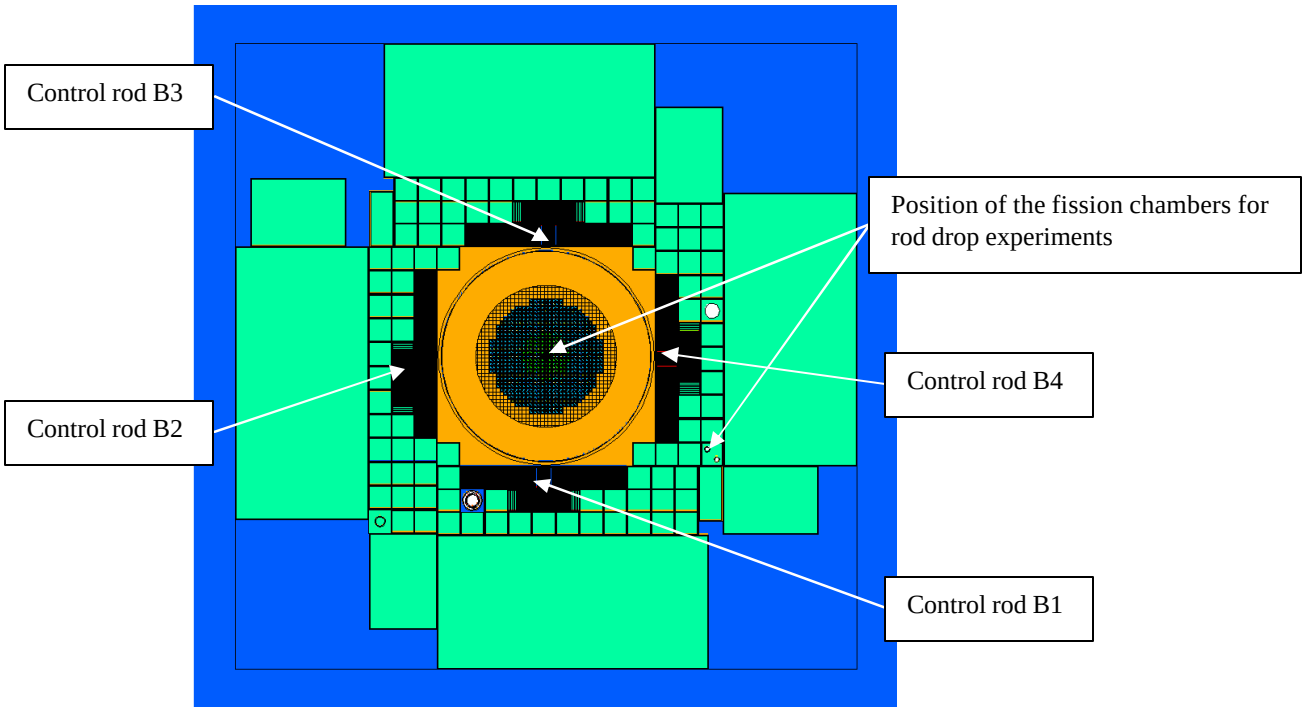

Figure 1: MCNP Mode1 of MINERVE Reactor with R1-MOX Loading (radial view)

2. Reactor Models

MCNP models of the R1-UO2 and R1-MOX core loadings for the MINERVE reactor were completed. They are detailed in reference [2]. Figure 1 shows the MCNP model of MINERVE for R1-MOX core loading.

3. Experimental Technique

3.1. Reactivity worth of the control rods

The total reactivity worth of the control rods is obtained in two steps. The first step is the measurement by the rod drop technique (using inverse kinetics equation method) [3] of the reactivity worth of the rod from the critical position down to the fully inserted position. The counting rate of a fission chamber positioned in the core is followed before, during and after the rod drop. A ^{235}U miniature fission chamber placed in the mid central cell was used for rod drop measurements in R1-UO2 and in R1-MOX. An additional equivalent ^{235}U chamber was also used in R1-UO2 and was placed inside graphite outside of the driver zone (see figure 1).

The second step is the measurement of the reactivity worth of the rod from the critical position up to the fully withdrawn position by asymptotic period technique, and then the Inhour equation of MINERVE in the given configuration of the core to translate the asymptotic period into reactivity. These methods were applied for each individual control rod, and for the combination of all four control rods.

3.2. Axial fission rates in R1-MOX

3.2.1. Axial profile of ^{237}Np and ^{235}U fission rates in the center of R1-MOX

The axial profile of ^{237}Np and ^{235}U fission rate in the central cell (oscillation cell) was studied using 4 mm diameter fission chambers. It was measured using a linear positioner system developed by CEA Cadarache that is based on a computer-driven system allowing accuracy better than 1mm on the position of the measured fission chamber.

3.2.2. Axial profile of total fission rate

The axial profile of the total fission rate in R1-MOX was obtained by integral gamma spectroscopy on irradiated fuel pins. The position of the two studied MOX pins (*MOX1* and *MOX 3*), located close to the central cell, is shown in figure 2. The gamma-spectroscopy device is made of a standard HPGe detector and electronics, with a lead collimation window allowing the measurement of the fuel pins with axial resolution of 2 cm or less.

3.3. Radial power profile in R1-MOX

Gamma spectroscopy measurements were also used to determine the relative power distribution (i.e. total fission rate distribution) inside the core configuration. It is accomplished in two steps. First the total fission rate radial profile in both MOX zone and UOx zone of the R1-MOX lattice is obtained by integral gamma-spectroscopy of the fuel pins. Then the power distribution inside R1-MOX was determined using the above measurements added to normalization measurements using single peak gamma-spectroscopy on ^{140}La gamma-ray at 1596.17 keV.

The gamma-spectroscopy device is similar to the one used for the axial profile of total fission rate, with a collimation window of 5 cm width allowing the investigation of the central part of each fuel pin. The location of the studied fuel pins is shown on figure 2. The fuel pins for power normalization are called *MOX1*, *MOX3*, *UOX7* and *UOX10*, from the central cell to the outer part of the lattice (see figure 2).

4. General Methodology

4.1. Reactivity worth of the control rods

4.1.1. Rod drop technique

Rod drop experiments are analyzed using inverse kinetics equations in the point model. Reactivity expressed in dollars is given by:

$$r_{\$}(t)=1+\Lambda^{*}\frac{\dot{c}(t)}{c(t)}-\Lambda^{*}\frac{e\hat{Q}(t)}{c(t)}-\sum_{j}a_{j}\frac{c(0)}{c(t)}e^{-l_{j}t}-\sum_{j}l_{j}a_{j}\int_{0}^{t}\frac{c(u)}{c(t)}e^{-l_{j}(t-u)}du$$

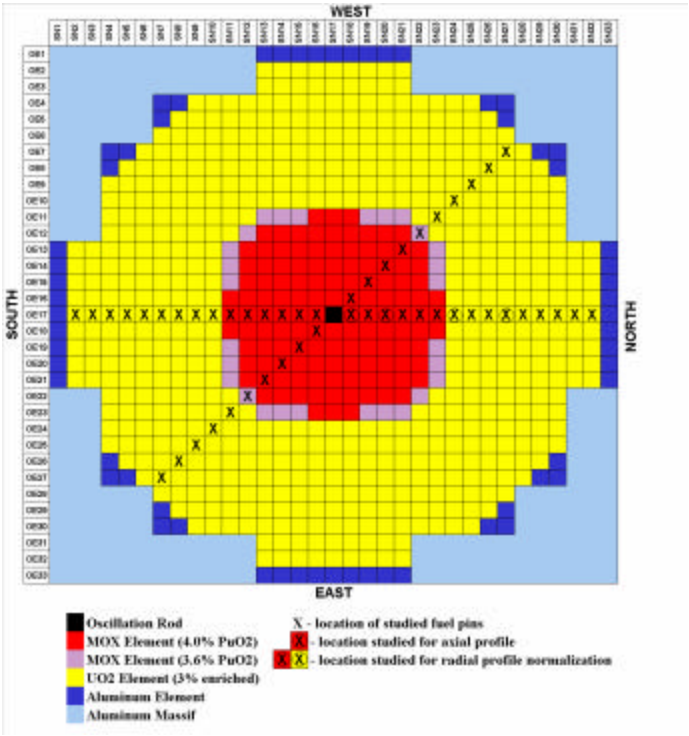

Figure 2: Locations of the Studied Fuel Pins for axial profile measurement

where $a_j = b_j/b$ are the effective relative yields and $\Lambda^* = \Lambda/b$ is the reduced generation time. The external/intrinsic source term $\Lambda^* e\,\hat{Q}/c(t)$ and the reactivity level at delayed critical are almost negligible even in the R1-MOX configuration.

An example of reactivity worth is illustrated on figure 3 for a control rod in the R1-MOX configuration. Uncertainty on the reactivity from the critical position is derived using the re-sampling technique and the uncertainties on a_j and λ_j [3]. The reactivity worth and their uncertainties are presented in section 5.2.

4.1.2. Reactivity excess measurement

Reactivity excess determination is performed by classical asymptotic period measurements and the Inhour relation. Counting rates are recorded on a ^{235}U miniature fission chamber positioned inside the core during divergence of the core. A short time interval after the complete withdrawal of the rod the counting rate follows a simple exponential increase Ae^{wt} which characterizes the reactor stable period $T = 1/w$.

Reactivity excess is deduced via the Inhour equation:

$$r = \Lambda^* w + \sum_j \frac{w\,a_j}{l_j + w}$$

where the notations are the same as in Section 4.1.1.

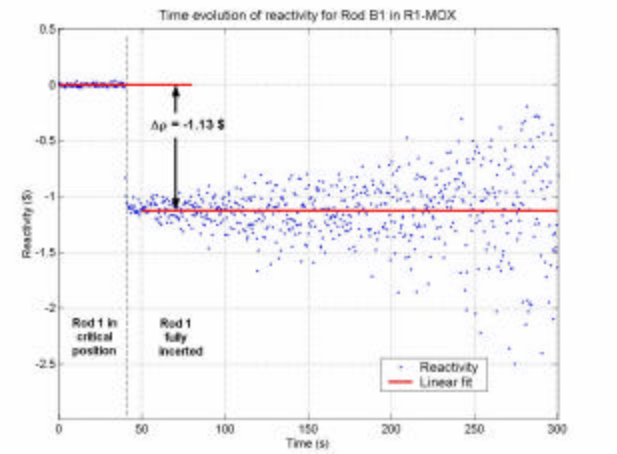

Figure 3: Example of reactivity worth determination using the rod drop technique

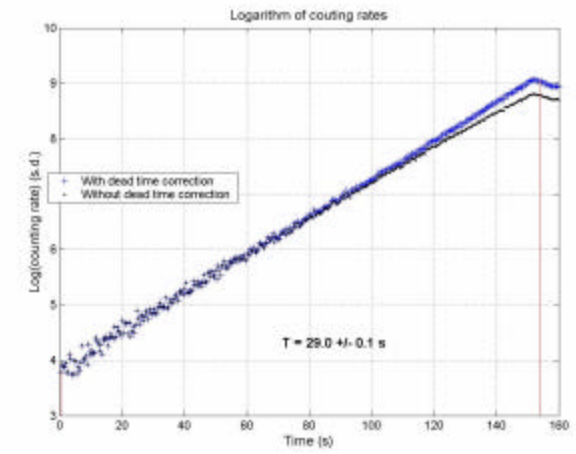

Figure 4: Example of stable reactor period adjustment

An example of ^{235}U miniature fission chamber signal during a divergence is given in figure 4. Uncertainties on the reactivity excess come from propagation of the uncertainties on the a_j and λ_j. Total rod reactivity worth, that is the sum of excess reactivity and the reactivity determined by rod drop, and their uncertainties are presented in section 5.2.

4.2 Axial fission rates

4.2.1. Axial fission rate with fission chambers

A miniature fission chamber is positioned in the center of the waterproof rod located in the central cell of the R1-MOX channel. It is positioned using the POLINE device (see Section 2.1.) with steps of 1 cm. Two measurements are performed for each axial position. The length of the measurements is selected so that the statistics on counting are better than 0.5%. A fission chamber located outside of the experimental zone (but inside the driver zone) and synchronized to the fission chamber in the central position, allows the normalization of all the measurements to the same power of the reactor. Finally, all the measured points are normalized to the measurement made in the mid plan of the core (this particular point is thus normalized to 1).

4.2.2. Axial total fission rate by gamma-scanning technique

The fuel pins are irradiated for 15 minutes at a power level of 40 Watts. After two hours of cooling, they are counted in the gamma scanning device by integral gamma-scanning. Each fuel pin is measured three times for each axial position. The device allows measurements of 2 cm segments over the entire length of the fuel pin (50 cm). A counting interval of 30 seconds is used so that the statistics are better than 0.5%. Synchronized to the counting of the studied fuel pin, another fuel pin (for normalization) is counted in order to correct the activity decay of gamma-rays.

In the end, all the measurements are normalized to the one made in the center of the fuel pin. The associated uncertainty is obtained by combining quadratically the uncertainty on the counting of each measurement, on the counting of the normalization pin and the uncertainty on the reproducibility of the measurement. Reproducibility is estimated by the standard deviation on three measurements in the same position for a given fuel pin.

4.3. Radial power profile

The measurements are aimed at determining the relative power (i.e. total fission rate) distribution inside the R1-MOX configuration. The measurements are performed in two steps.

First, the radial profile of the total fission rate in both MOX zone and UOx zone of the R1-MOX lattice was obtained by integral gamma-spectroscopy on fuel pins. This specific measurement used exactly the same technique as for the axial fission rate measurements. Then the power distribution was obtained using the above measurements added to normalization measurements using single peak gamma-spectroscopy on ^{140}La. ^{140}La is a fission product created after irradiation of the fuel pins, through the following decay scheme:

$$^{140}\mathrm{Ba} \xrightarrow{b^- \; T=12.74\,d} {}^{140}\mathrm{La} \xrightarrow{b^- \; T=1.68\,d} {}^{140}\mathrm{Ce}$$

After resolution of the equations of evolution of ^{140}La during the irradiation, cooling and measurement phases, one can show that the total fission rate inside a fuel pin can be written as follows:

$$F = \frac{(l_L - l_B)\times N_L}{Y_B \times g_L \times h_L \times f_L} \times \frac{T_c}{T_r} \Big/ \left(\frac{l_L}{l_B} e^{-l_B T_o} \left(1 - e^{-l_B T_i}\right)\left(1 - e^{-l_B T_c}\right) - \frac{l_B}{l_L} e^{-l_L T_o} \left(1 - e^{-l_L T_i}\right)\left(1 - e^{-l_L T_c}\right)\right) \quad \textbf{(1)}$$

where T_i is the irradiation time, T_0 is the cooling time, T_c is the counting time, T_r is the net time of the counting (i.e. (T_c – Tm) where Tm is the dead time of the electronic chain), λ_i are decay constants for isotope i, N_L is the integral counting of the studied gamma-ray of ^{140}La, f_L is the self-absorption of ^{140}La gamma-ray at 1596.17 keV inside the fuel pin, g_L is the intensity of the gamma-ray of ^{140}La at 1596.17 keV and Y_B is the effective fission yield of ^{140}Ba.

The associated uncertainty, derived by the quadratic sum of all uncertainties, can be written as:

$$\left(\frac{\Delta F}{F}\right)^2 = \left(\frac{\Delta N}{N}\right)^2 + \left(\frac{\Delta Y_B}{Y_B}\right)^2 + \left(\frac{\Delta f_L}{f_L}\right)^2 + K_L{}^2 \times (\Delta l_L)^2 + K_B{}^2 \times (\Delta l_B)$$

with:

$$K_L{}^2 = \left\{ \frac{1}{l_L - l_B} - \left[\begin{array}{l} \dfrac{e^{-l_B \times T_o}}{l_B}\left(1 - e^{-l_B \times T_i}\right)\left(1 - e^{-l_B \times T_c}\right) \\ + \dfrac{l_B}{l_L{}^2} e^{-l_L \times T_o}\left(1 - e^{-l_L \times T_i}\right)\left(1 - e^{-l_L \times T_c}\right) \\ + \dfrac{l_B \times T_o}{l_L} e^{-l_L \times T_o}\left(1 - e^{-l_L \times T_i}\right)\left(1 - e^{-l_L \times T_c}\right) \\ - \dfrac{l_B \times T_i}{l_L} e^{-l_L \times T_o} \times e^{-l_L \times T_i}\left(1 - e^{-l_L \times T_c}\right) \\ - \dfrac{l_B \times T_c}{l_L} e^{-l_L \times T_o} \times e^{-l_L \times T_c}\left(1 - e^{-l_L \times T_i}\right) \end{array} \right] \Big/ \frac{C \times (l_L - l_B) \times T_c}{F \times Y_B \times f_L \times T_r} \right\}^2$$

$$K_B^2 = \left\{ \frac{1}{l_L - l_B} - \left[\begin{array}{l} \frac{e^{-l_L \times T_o}}{l_L}\left(1 - e^{-l_B \times T_i}\right)\left(1 - e^{-l_B \times T_c}\right) \\ + \frac{l_L}{l_B^2} e^{-l_B \times T_o}\left(1 - e^{-l_B \times T_i}\right)\left(1 - e^{-l_B \times T_c}\right) \\ + \frac{l_L \times T_o}{l_B} e^{-l_B \times T_o}\left(1 - e^{-l_{BL} \times T_i}\right)\left(1 - e^{-l_B \times T_c}\right) \\ - \frac{l_L \times T_i}{l_B} e^{-l_B \times T_o} \times e^{-l_B \times T_i}\left(1 - e^{-l_B \times T_c}\right) \\ - \frac{l_L \times T_c}{l_B} e^{-l_B \times T_o} \times e^{-l_B \times T_c}\left(1 - e^{-l_B \times T_i}\right) \end{array} \right] / \frac{C \times (l_L - l_B) \times T_c}{F \times Y_B \times f_L \times T_r} \right\}^2$$

Knowing the total fission rate inside the 2 studied MOX pins and the 2 studied UOx pins, it is possible to determine normalization factors for MOX and UOx as follows:

$$r_{MOX} = 2 \times \frac{F_{MOX1} + F_{MOX3}}{F_{MOX1} + F_{MOX3} + F_{UOX7} + F_{UOX10}}$$

$$r_{UOX} = 2 \times \frac{F_{UOX7} + F_{UOX10}}{F_{MOX1} + F_{MOX3} + F_{UOX7} + F_{UOX10}}$$

with:

$$\left(\frac{(\Delta r_{MOX})}{r_{MOX}}\right)^2 = (r_{MOX})^2 \times \left[\frac{\left(\sum_i F_{UOX,i}\right)^2}{\left(\sum_i F_{MOX,i}\right)^2} \times \left(\sum_i \left(\frac{\Delta F_{MOX,i}}{F_{MOX,i}} \right)^2 \right) + \sum_i \left(\frac{\Delta F_{UOX,i}}{F_{UOX,i}} \right)^2 \right]$$

$$\left(\frac{(\Delta r_{UOX})}{r_{UOX}}\right)^2 = (r_{UOX})^2 \times \left[\frac{\left(\sum_i F_{MOX,i}\right)^2}{\left(\sum_i F_{UOX,i}\right)^2} \times \left(\sum_i \left(\frac{\Delta F_{UOX,i}}{F_{UOX,i}} \right)^2 \right) + \sum_i \left(\frac{\Delta F_{MOX,i}}{F_{MOX,i}} \right)^2 \right]$$

These normalization factors are applied to all measurements performed by integral gamma-scanning inside MOX and UOx fuel pins regions of the experimental zone. Based on equation 1, the terms g_L and η_L will disappear in the expression of r_{MOX} and r_{UOx}. Therefore, only the ratios of gamma-ray shielding factors and effective fission yields appear in the equation which means that it is not necessary to know the absolute values of these terms. The method to calculate f_L and Y_B (the gamma-ray shielding factor and the effective fission yield) is fully detailed in reference [2] [4].

Table 1 shows the results of gamma-ray shielding factors in the case of the 4 studied fuel pins, for gamma-ray of ^{140}La at 1596.17 keV.

Table 2 presents the values of the effective fission yields of ^{140}Ba (based on ENDF-BVI data library) for the 4 studied fuel pins.

Table 1
Gamma-Ray Shielding Factors for MINERVE R1-MOX Fuel Pins

	La-140	s.d. (%)
MOX 1	0.936	1.53 %
MOX 3	0.936	1.56 %
UOX 7	0.935	1.13 %
UOX 10	0.935	1.02 %

Table 2
Effective Fission Yields of Ba-140 in MINERVE R1-MOX Fuel Pins

	Y_B	s.d. (%)
MOX 1	0.0550	1.04%
MOX 3	0.0532	1.06%
UOX 7	0.0618	0.91%
UOX 10	0.0619	0.93%

5. Experimental Results

5.1. Reactivity worth of the control rods

Tables 3, 4 and 5 present the experimental results of the reactivity worth of control rods in R1-UO2 and R1-MOX. The reactivity worth obtained by rod drop from the critical positions and the total reactivity worth (the sum of the previous one and of the excess reactivity of the core) are presented.

Tables 3 and 4 show that the experimental results strongly depend on the position of the fission chamber. It can be explained by a systematic bias on the measurements, called MSM (Modified Source Multiplication) factors that take into account spatial and energetic corrections due to the rod drop, at the exact location of the fission chamber [3]. In equations, the use of the MSM factors can be formalized as follow:

$$r_1 = \frac{R_0}{R_1} r_0 \times \underbrace{\frac{e_1 \times S_{eff,1}}{e_0 \times S_{eff,0}}}_{MSM\ \ correction},$$

where ρ_0 is the antireactivity of a reference state to which corresponds a counting rate R_0 in the detector, ρ_1 is the antireactivity of the studied state to which corresponds a counting rate R_1, and

$$e = \frac{\langle \Sigma_d | \Phi \rangle}{\langle j^* | F\Phi \rangle} \text{ and } S_{eff} = \langle j^* | S \rangle$$

are respectively the detector efficiency and the effective source, where Σ_d is the cross section of the detector, Φ is the flux, F is the fission operator and j^* is the adjoint flux in the critical state. Note that the difference on the reactivity excess of the core between the two experiments is simply due to a variation of the water temperature in the core. Further investigation is presented in section 6.2.

Table 3
Reactivity worth ($) of control rods in R1-UO2 obtained with ^{235}U fission chamber in the central cell of the core

Case	From critical positions	Total
Rod B1	1.00 ± 0.06	1.18 ± 0.06
Rod B2	1.14 ± 0.06	1.32 ± 0.06
Rod B3	1.22 ± 0.07	1.40 ± 0.07
Rod B4	1.14 ± 0.08	1.32 ± 0.08
All rods*	5.44 ± 0.43	5.62 ± 0.43

*rod B3 in the critical position, all others fully withdrawn

Table 4
Reactivity worth ($) of control rods in R1-UO2 obtained with ^{235}U fission chamber in graphite outside of the driver zone

Case	From critical positions	Total
Rod B1	1.14 ± 0.06	1.37 ± 0.06
Rod B2	1.02 ± 0.06	1.25 ± 0.06
Rod B3	1.29 ± 0.07	1.52 ± 0.07
Rod B4	1.32 ± 0.08	1.55 ± 0.08
All rods*	7.75 ± 0.43	7.98 ± 0.43

*rod B3 in the critical position, all others fully withdrawn

Table 5
Reactivity worth ($) of control rods in R1-MOX

Case	From critical positions	Total
Rod B1	1.13 ± 0.06	1.34 ± 0.06
Rod B2	1.30 ± 0.09	1.51 ± 0.09
Rod B3	1.39 ± 0.08	1.60 ± 0.08
Rod B4	1.06 ± 0.06	1.27 ± 0.06
All rods*	7.04 ± 0.36	7.25 ± 0.36

*rod B3 in the critical position, all others fully withdrawn

5.2. Axial fission rates

Figure 5 shows the experimental results for axial fission rate profiles of ^{237}Np and ^{235}U. There is excellent agreement of the two results in the fuel zone of the pin where the fundamental mode, and thus a cosine shape, is established. Above and below the fuel zone, effects due to Plexiglas spacers are seen by the ^{235}U chamber but not by the ^{237}Np chamber. This is because of the threshold fission cross section of ^{237}Np.

The results of the measurements by integral gamma-spectroscopy on fuels pins MOX1 and MOX3 are shown in figure 6. The measurements show excellent accuracy (better than 1%) for all points including reproducibility of the experiment (each point is the mean of three measurements).

Fitting all of the measured axial profiles in the range [-20 cm ;+20 cm] (i.e. inside the fuel zone of the pins) with a cosine function $\cos(B_z \times z)$, the axial bucklings are obtained as shown in Table 6.

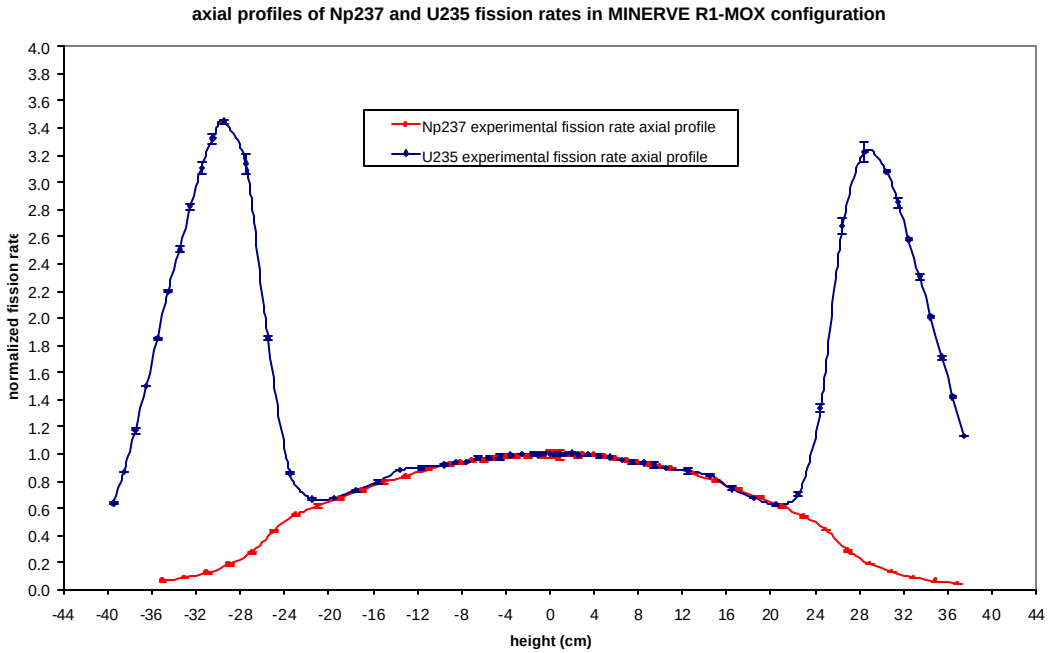

Figure 5: axial distribution of ^{237}Np and ^{235}U fission rate

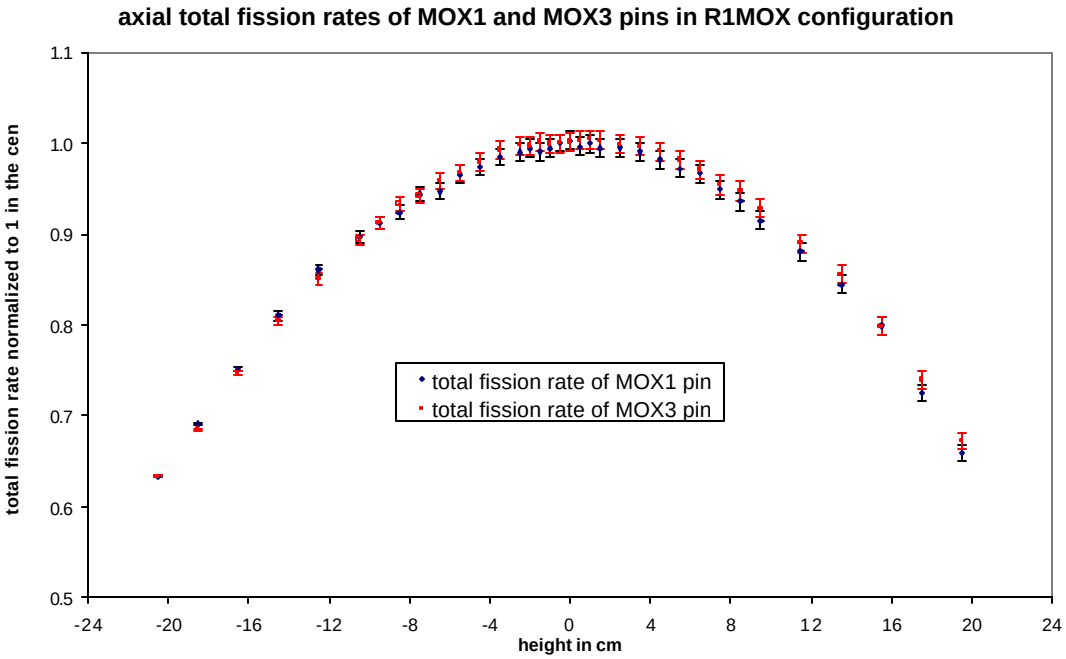

Figure 6: axial total fission rate of *MOX1* and *MOX3* pins

Table 6 Axial buckling in R1-MOX	
Experiment	B_z^2 (cm^{-2})
Total fission rate on MOX1	$1.86 \times 10^{-4} \pm 3.0 \times 10^{-6}$
Total fission rate on MOX3	$1.88 \times 10^{-4} \pm 2.0 \times 10^{-6}$
^{235}U fission rate in the center of R1-MOX	$1.89 \times 10^{-4} \pm 4.0 \times 10^{-6}$
^{237}Np fission rate in the center of R1-MOX	$1.88 \times 10^{-4} \pm 3.0 \times 10^{-6}$

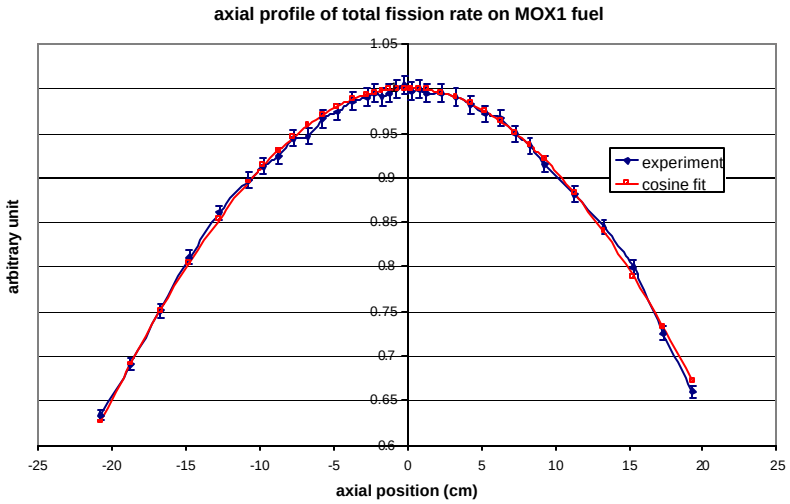

Figure 7: axial profile of MOX1 pin and cosine fit

The results show very good agreement between the two pins, and with the fission chamber measurements (with a standard deviation on the axial buckling of 0.65%). An example of the agreement between experimental values and the cosine fitting curve is given in figure 7.

5.3. Radial power profile in R1-MOX

Figure 8 shows an example of the measured gamma-ray of ^{140}La at 1596.17 keV for *MOX1* fuel pin. Note that in the case of MOX pins, this peak is disturbed by the 2nd escape peak of ^{208}Tl at 2614.5 keV, coming from decays of ^{240}Pu. These two peaks have to be uncorrelated (gaussian uncorrelation) as shown in figure 8. In the case of UOx pins, no ^{208}Tl peak appears as there is no ^{240}Pu inside the pins.

After treatment of all the experimental data and using the effective fission yields and shielding factors of Section 4.3, the following power normalization factors are obtained:

$$r_{MOX} = 0.500 \quad (\pm 1.7\%)$$
$$r_{UOX} = 0.500 \quad (\pm 1.7\%)$$

The equality of the two factors is a coincidence. Figures 9 and 10 show experimental results with errorbars at 1 standard deviation. The distribution is relative to the location of studied fuel pins described in Section 3.3.

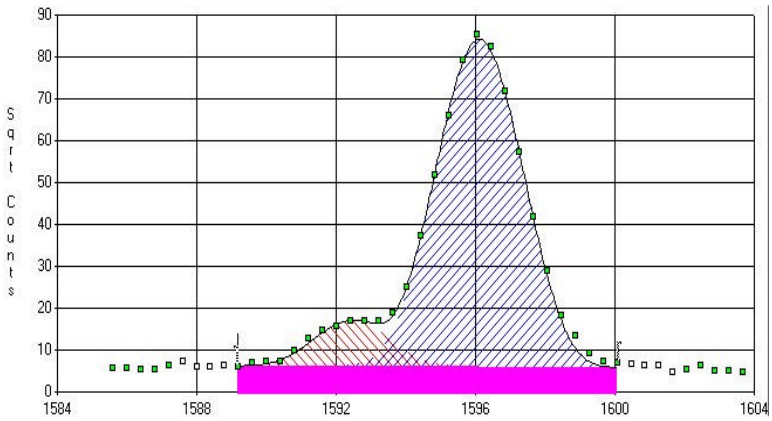

Figure 8: ^{140}La at 1596.17 keV and 2nd escape ^{208}Tl peak for MOX1 fuel pin – counts vs. energy

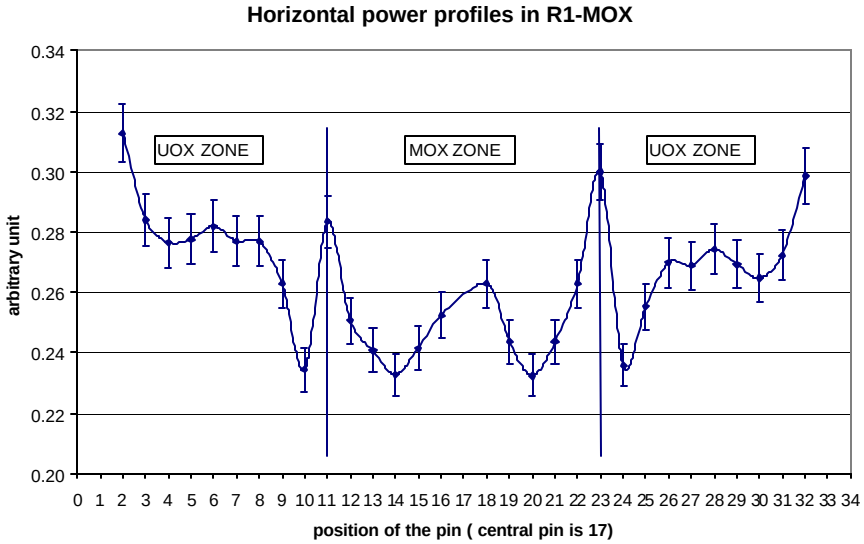

Figure 9: Horizontal radial power distribution in R1-MOX configuration

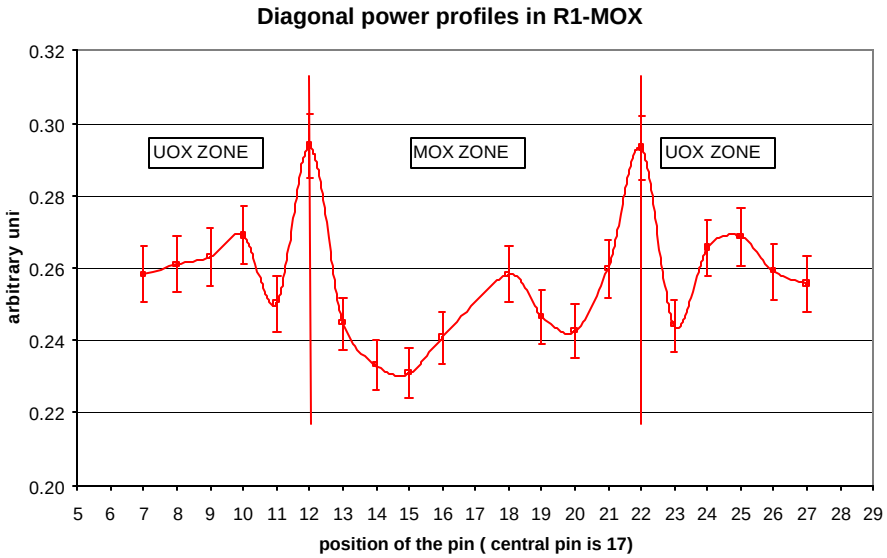

Figure 10: Diagonal radial power distribution in R1-MOX configuration

Accuracies better than 3% were obtained for the measurements. In every case, a slight asymmetry around the central cell is observed. It comes from the fact that the oscillation rod that was introduced in the central zone during the experiment was not perfectly centered which induces an asymmetry of the water blade around this rod.

The power profile at the interface between the MOX and UO2 regions is also well reproduced and comes from the fact that the neutron spectrum is harder in MOX cells than in UO2 cells due to resonances in the absorption cross sections of plutonium isotopes.

Finally, the asymmetry of the power between the south region of the lattice and north region of the lattice is due to the asymmetry on the loading of the driver zone.

6. Calculational Results

6.1. Multiplication factors

Table 7 shows the results of calculations of the multiplication factor for R1-MOX with Monte Carlo codes MCNP-4C2 (with ENDF-BVI), and in R1-UO2 with Monte Carlo codes MCNP-4C2 (with ENDF-BVI) and TRIPOLI4 (with JEF2.2).

The results depend primarily on the data library (JEF2.2 or ENDF-BVI) but also on the Monte Carlo code (TRIPOLI4 or MCNP4C2). The consistency with the experimental multiplication factor from reactivity excess measurements is verified in every case within approximately \$1 (0.0070). With JEF2.2, the difference between TRIPOLI4 and MCNP4C2 results is around is about \$0.7 in R1-UO2.

With MCNP, the effect on the data library is about \$1.7 for both R1-MOX and R1-UO2 cases and can be explained by differences in the cross sections of Al-27 and U-235 between JEF2.2 and ENDF-BVI. As an illustration, Table 8 shows results with MCNP4C2 + ENDF-BVI changing only the Al-27 cross section into JEF2.2. It also shows results in R1-UO2 obtained with TRIPOLI4 + JEF2.2, using Al-27, U-235 and (Al-27 + U-235) cross sections from the JEFF3 library.

A positive effect of about \$1.3 is observed in the MCNP4C2 calculations from changing the Al-27 cross-section from ENDF-BVI to JEF2.2. This occurs for both R1-UO2 and R1-MOX core loadings. In the same manner, an important negative effect of about \$1 is observed in the TRIPOLI4 calculations from changing the Al-27 cross-section from JEF2.2 to the new JEFF-3 data library.

In conclusion, the strong impact of Al-27 cross section choice has to be noticed. Further investigation is being performed with new JEFF3 and ENDF-BVII data libraries, and by reviewing past integral experiments on Al-27.

Table 7
Multiplication factor with all rods withdrawn

	MCNP4C2 + ENDF-BVI		MCNP4C2 + JEF2.2		TRIPOLI4 + JEF2.2		Experiment	
case	keff	s.d.	keff	s.d.	keff	s.d.	keff	s.d.
R1-UO2	0.99090	0.00025	1.00304	0.00025	1.00761	0.00010	1.00147	0.00005
R1-MOX	0.99467	0.00025	1.00631	0.00014	/	/	1.00140	0.00005

Table 8
Effect of Al-27 and U-235 cross sections

	MCNP4C2 + Al-27 from JEF2.2		TRIPOLI4 + U-235 from JEFF3		TRIPOLI4 + Al-27 from JEFF3		TRIPOLI4 (Al-27 + U-235) from JEFF3	
	keff	s.d.	keff	s.d.	keff	s.d.	keff	s.d.
R1-UO2	0.99982	0.00026	1.00501	0.00010	1.00070	0.00010	0.99866	0.00010
R1-MOX	1.00431	0.00017	/	/				

6.2. Reactivity worth of the rods

Tables 9 and 10 show the calculated reactivity worth of all rods using MCNP4C2 with ENDF-BVI cross-sections. Calculational values are also compared to the experimental results.

In the case where the U-235 fission chamber is placed in the center of the core, there is a discrepancy of about 10 % to 15 % between calculation and experiments for each rod for both R1-UO2 and R1-MOX core loadings. The discrepancy increases to around 40% for the case of all the rods together. This proves that the spatial/energetic corrections to be applied to experiments (MSM factors, see Section 5.2) are important and need to be made in the future. The MSM factors also take into account the modification of the source (external and intrinsic) and of the efficiency of the fission chamber during the rod drop.

In the case where the U-235 fission chamber is placed in the graphite reflector zone, discrepancies between calculations and experiments are less than 8 % within 2 standard deviations. This tends to show that energetic and spatial corrections are weak in the position of the fission chamber. This is corroborated by the fact that the chamber is located far from the external and intrinsic sources, and that the neutron spectrum at the chamber position is weakly affected by the rod drop as the chamber is inside the graphite reflector zone. Nevertheless, further investigation and calculations of MSM factors need to be performed in the future to identify and explain these discrepancies.

Discrepancies between data libraries have been noted for the cross sections and resonance parameters of hafnium [5]. This also requires further study, in particular calculations using new data libraries need to be performed. A related program, called OCEAN – Oscillation in Core of samples containing Neutron Absorbers, will address these issues since individual isotopes of hafnium and other absorbers will be investigated. The OCEAN program will begin in 2005.

Table 9
Calculated Reactivity Worth ($) of Control Rods in R1-UO2

	MCNP4C2 + ENDF-BVI	^{235}U fission chamber in the center of the core	^{235}U fission chamber in reflector zone
Case	Total	(C-E)/E	(C-E)/E
Rod B1	1.32 ± 0.05	12.6 %	-3.6 %
Rod B2	1.32 ± 0.05	0.1 %	5.7 %
Rod B3	1.64 ± 0.05	17.4 %	7.6 %
Rod B4	1.44 ± 0.05	9.2 %	-6.8 %
All rods*	7.70 ± 0.05	37.1 %	-3.5 %

*rod B3 in the critical position, all others fully withdrawn

Table 10
Calculated Reactivity Worth ($) of Control Rods in R1-MOX obtained with MCNP4C2 + ENDF-BVI (^{235}U fission chamber in the center of the core)

Case	Total	(C-E)/E in %
Rod B1	1.56 ± 0.05	16.8 %
Rod B2	1.70 ± 0.05	12.5 %
Rod B3	1.88 ± 0.05	17.5 %
Rod B4	1.55 ± 0.05	22.2 %
All rods*	10.26 ± 0.05	41.6 %

*rod B3 in the critical position, all others fully withdrawn

6.3. Axial fission profile

Axial ^{235}U and ^{237}Np fission rates have been computed with MCNP4C2 using ENDF-BVI cross-sections. They are illustrated in Figures 11 and 12. Excellent agreement is found for the Np-237 axial fission rate profile. In the fuel zone, the agreement is also very good in the case of the U-235 axial fission rate. Outside of the fuel region, the inner region contains plexiglass spacers. The effect due to the plexiglas spacers is observed but is not well calculated. This is most likely due to the uncertainty on the size and composition of the spacers.

Axial bucklings deduced from cosine fits in the fuel region are presented in Table 11. Very good agreement between calculated and experimental buckling is found in the case of Np-237. Axial buckling with U-235 is also in agreement within experimental standard deviation and statistical standard deviation on the Monte Carlo calculation.

Table 11
Calculated axial buckling in R1-MOX

Case	B_z^2 (cm^{-2})
^{235}U fission rate in the center of R1-MOX	$1.70\text{x}10^{-4} \pm 2.5\text{x}10^{-5}$
^{237}Np fission rate in the center of R1-MOX	$1.89\text{x}10^{-4} \pm 9.0\text{x}10^{-6}$

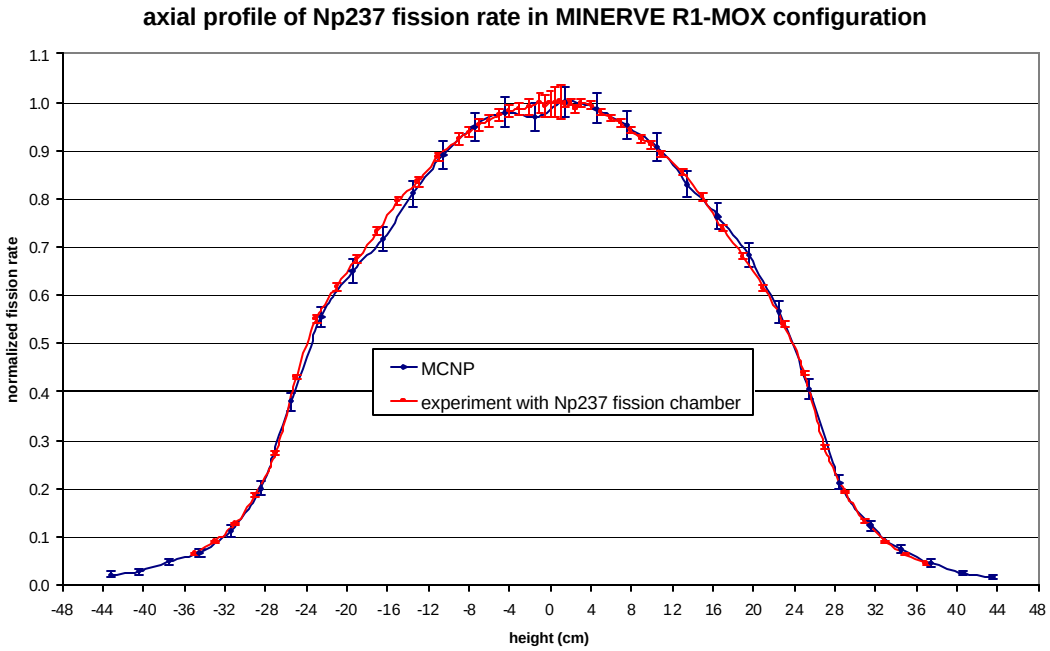

Figure 11: comparison of calculated and measured axial profile of Np-237 fission rate in R1-MOX

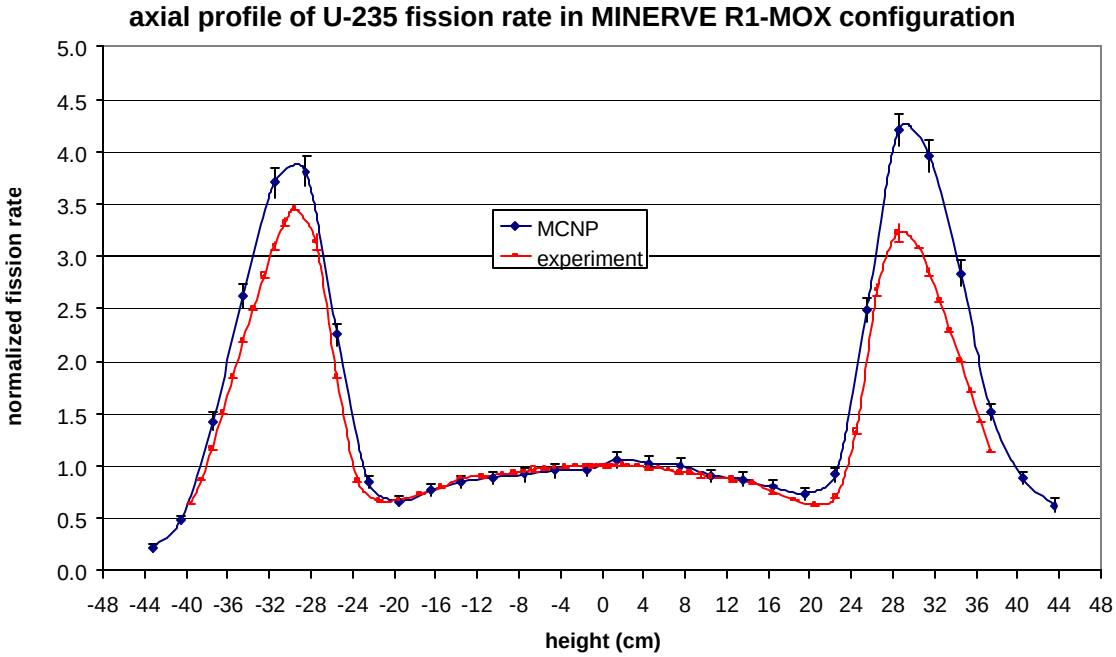

Figure 12: comparison of calculated and measured axial profile of U-235 fission rate in R1-MOX

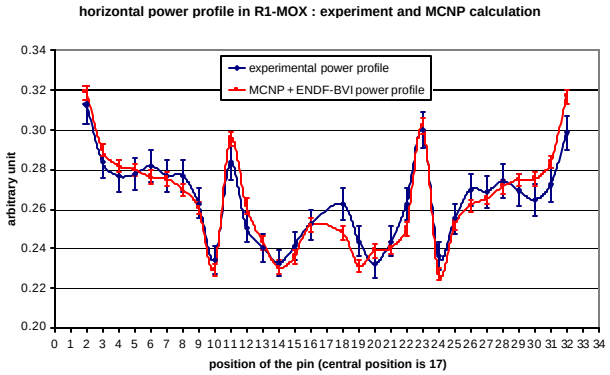

Figure 13: Comparison of calculated to experimental horizontal power profile in R1MOX

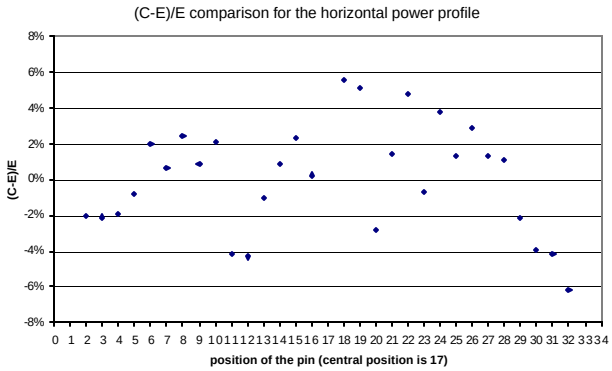

Figure 14: (C-E)/E in the horizontal direction

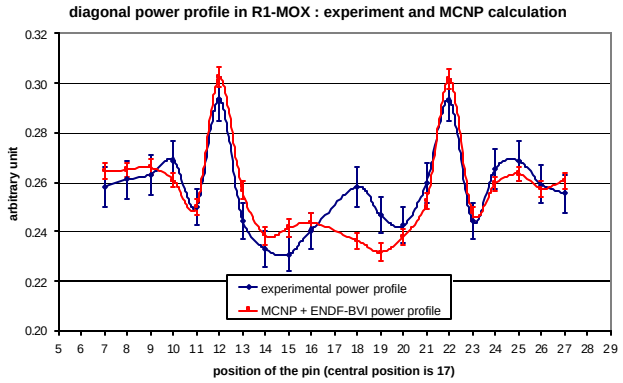

Figure 15: Comparison of calculated to experimental diagonal power profile in R1MOX

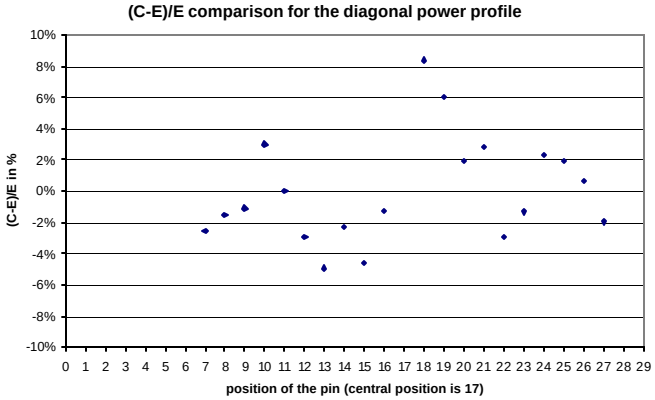

Figure 16: (C-E)/E in the diagonal direction

6.4. Radial power profile

Figures 13, 14, 15 and 16 show the comparison of calculated radial power profiles to experimental measurements in both horizontal and diagonal directions (see Section 3.2.2). Good agreement is observed in all cases as nearly all points are consistent within two standard deviations. However, a slight discrepancy between calculation and experiments is shown near the central cell. It was experimentally explained by an asymmetry on the loading of the oscillation rod in the central cell (i.e. position number 17). For fuel pins not close to the central cell (more than 3 cells from it), the discrepancy between calculation and experiments is better than 4%.

Finally, the power profile over the whole experimental lattice of R1-MOX was calculated and is shown in figure 17.

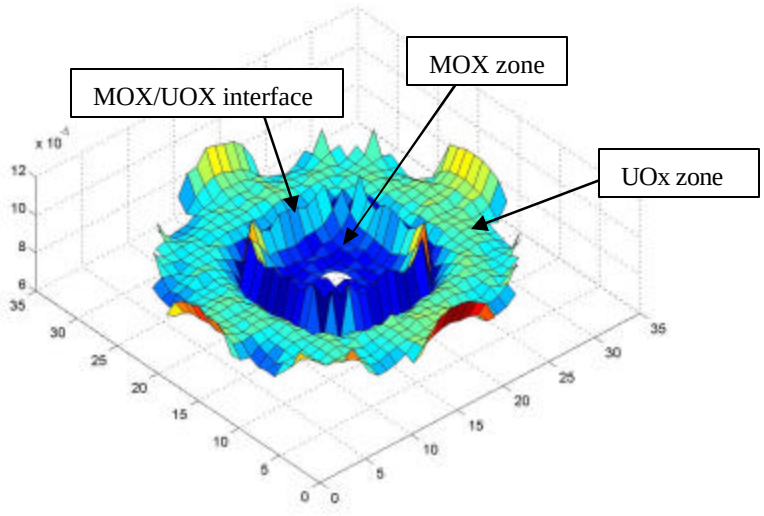

Figure 17: power profile in R1-MOX configuration, obtained by MCNP calculation

7. Conclusions

This paper described the experimental results of safety parameters measurements in R1-UO2 and R1-MOX configurations of the MINERVE facility. It also compared the results to calculations performed with the MCNP code with JEF2.2 and ENDF-BVI data libraries, and with the TRIPOLI4 code with JEF2.2.

The consistency of calculation of the multiplication factor with the experiment for both R1-UO2 and R1-MOX was within about \$1. The strong impact of the Al-27 cross section on the calculation results was shown and explained the discrepancy between results with ENDF-BVI (underestimation of the experimental multiplication factor) and with JEF2.2 (overestimation of the experimental multiplication factor).

Agreement better than 8 % was obtained in R1-UO2 for the reactivity worth of the hafnium control rods in the case where the fission chamber used for the experiments was placed outside the driver zone inside the graphite reflector zone. When the fission chamber was placed in the central cell, a discrepancy between calculation and experiments of 10% to 15% was found for each control rod. A 40% discrepancy was observed for the case of all rods fully inserted. Further investigation is necessary to take into account MSM factors, i.e. to take into account the modification of the source (external/intrinsic) and of the efficiency of the chamber during the rod drop measurements.

Very good agreement between calculation and experiment was found on the axial profile of Np-237 fission rate in R1-MOX and on the axial buckling. Good agreement was also observed in the fuel region of the studied pins for the axial fission rate of U-235. A slight discrepancy was observed outside of the fuel region due to the plexiglass spacers.

An agreement between calculation and experiment better than 6% (i.e. within 2 standard deviations) was shown for the radial power profile in the R1-MOX loading, in spite of the asymmetry observed on the loading of the oscillation rod in the central cell. For fuel pins not close to the central cell (more than 3 cells away from it), the discrepancy between calculation and experiments was better than 4%.

These initial results show that the MCNP and TRIPOLI4 models developed for the R1-UO2 and R1-MOX configurations of the MINERVE facility give consistent results with the experimental results for most of the safety parameters that have been measured.

Acknowledgements

The authors of this paper thank all the participants to the experimental program and their industrial partners for their financial support and in particular Electricité de France (EDF) and the U.S. Department of Energy.

References

1. J.P. Hudelot, R. Klann, P. Fougeras, F. Jorion, N. Drin, L. Donnet, OSMOSE: An Experimental Program for the Qualification of Integral Cross Sections of Actinides, Proceedings of the PHYSOR-2004 Topical Meeting, April, 2004.

2. R. Klann, JP. Hudelot, M. Antony, B. Micklich, G. Perret, N. Thiollay, G. Imel, JM. Girard, V. Laval, MINERVE Reactor Characterization in Support of the OSMOSE Program: Spectral Indices, Proceedings of the PHYSOR-2004 Topical Meeting, April, 2004.

3. G. Perret, C. Jammes, G. Imel, C. Destouches, P. Chaussonnet, JM. Laurens, R. Soule, GM. Thomas, W. Assal, P. Fougeras, P. Blaise, JP. Hudelot, H. Philibert, G. Bignan, Determination of reactivity by a revised rod drop technique in the MUSE4 programme – Comparison with dynamic measurements, 7th IEM, Jeju, Korea, 2002.

4. JP. Hudelot, P. Fougeras, S. Cathalau, Measurement of the modified conversion ratio of ^{238}U by gamma-ray spectrometry on an irradiated fuel pin, CGS11 conference, Prague, September 2002.

5. JM. Palau, Current status and proposals concerning Hf evaluated nuclear data, for JEFF3, JEF/DOC-924.